Growth of Fractal Fault Patterns

A. Sornette,[1] P. Davy,[2] and D. Sornette[1]
[1]*Laboratoire de Physique de la Matière Condensée, Faculté des Sciences, Parc Valrose, 06034 Nice CEDEX, France*
[2]*Centre Armoricain d'Etude Structurale des Socles, Université de Rennes 1, 35042 Rennes CEDEX, France*
(Received 9 January 1990)

Experiments on the formation of faults in a laboratory model of the Earth's crust are presented; they respect its vertical rheological stratification, a brittle layer on top of ductile layers. As a result of the competition between the different nature of the brittle- and ductile-layer deformations, complex fractal patterns of faults are formed with fractal dimension 1.70 ± 0.05 independent of the fault densities associated with different brittle-ductile coupling. We propose a kinematic formulation of the mechanical problem which suggests an analogy with previously studied fractal-growth problems.

PACS numbers: 62.20.Mk, 91.35.Gf, 91.45.−c, 91.60.Ba

Since the introduction of the model of diffusion-limited aggregation[1] (DLA), considerable interest has developed in a wide variety of growth phenomena.[2,3] More recently, rupture has been studied from the point of view of "fractal growth."[4-6] In most of the rupture problems which have been considered, a crack is irreversibly formed when the stress applied to a given portion of the system exceeds its rated rupture threshold. Once failed, the cracked domain cannot sustain stress anymore. As a consequence, screening and enhancement effects occur on large defects and can have a long range. Crack growth patterns[4-6] can thus be related to those appearing in so-called Laplacian growth processes.[1-3]

However, in nature, most systems present a greater complexity. First, cracks can propagate in mode II (shear) or III (torsion) and can still support important stresses after their formation (in this case, we call them faults). Second, the constitutive material laws often deviate from pure elastic to plastic with irreversible deformations. Third, cracks often do not propagate in directions parallel to the plane of maximum deviatoric shear stress. This leads to a breakdown of coaxiality between the applied stress tensor and the resulting strain tensor[7] and to the formation of complex crack patterns[8] which depend on the material, on the boundary conditions, and on the nature of the solicitations.[9]

In this Letter, we introduce a novel general quasi-two-dimensional mechanical model of crack pattern formation which exhibits fractal rupture patterns. This model is inspired from the structure of the Earth's crust and mantle and its dynamics is thought to represent a simplified version of plate tectonics.[10-12] It consists of a brittle layer (dry sand with Mohr-Coulomb frictional law with a friction coefficient $k \approx 0.6$) lying on top of ductile layers (silicone putties and golden syrup) which are submitted to various strain fields and different boundary conditions. Its main novelty is that it addresses a regime of *very large imposed deformations*. In this regime, the growth of the fault patterns is controlled by the compatibility of in-plane deformations which produce long-range correlated displacements. The large deformations are accomodated by (1) the creation of antithetic and synthetic faults and (2) rotations of faults and blocks (because of its kinematic resemblance to the tilting of a row of books on a shelf, this tectonic process is usually referred to as a "bookshelf" mechanism[13]). One can thus trace back the origin of the fractal fault structure to the long-range correlations of the in-plane deformations introduced by our choice of boundary conditions (see below).

By varying the ductile-layer viscosities, we have investigated a large range of rheologies and corresponding fault patterns. For loose boundary conditions allowing long-range propagation of strain, we observe fractal fault patterns with fractal dimension $D_f = 1.70 \pm 0.05$. A remarkable result is the independence of D_f with respect to the ductile-layer viscosities. On the other hand, the distribution of fault lengths, which seems to exhibit a power-law dependence over a limited range, is sensitive to the rheology.

In one set of experiments reported here, a wedge of rectangular shape and transverse dimension ≈ 20 cm penetrates at constant velocity $U = 5$ cm/h into the system (of size 40 cm × 68 cm) from the southern side. The other sides are confined by rigid walls, except the eastern side which is kept free. The upper brittle layer is made of quartz uncemented sand of aeolian origin from Fontainebleau (France). Sieving retains the fraction below 0.2 mm. The layer fails according to a Mohr-Coulomb frictional law (rupture occurs in a given plane when the shear stress along this plane exceeds the normal stress times a friction coefficient k), and presents a negligible cohesion. Shear failure occurs along faults (in fact, narrow shear bands) where progressive dilation causes strain softening and hence localization of the strain. The lower layers are made of two silicone putties of different viscosity η (from 0.5×10^4 to 7×10^4 Pas) and density (from 1.2 to 1.35). The basic material is Gomme 7007, manufactured by Rhone-Poulence, France. It is perfectly Newtonian at the experimental strain rates (less than 10^{-4} s^{-1}). The three layers float on a thick layer of golden syrup which ensures a free boundary condition at the bottom of the silicone layers (see Fig. 1 for the values of the thickness, density, and viscosity of the different layers).

The indentation is accommodated (see Fig. 1) by

thickening in front of the indenter and by eastward lateral escape towards the free boundary. Except in front of the indenter, the deformation generates a pattern of vertical faults with horizontal shear components (mode II). In this region, the strain field is quasibidimensional and propagates throughout the system ensuring long-range correlations. In this Letter, we focus on the geometry and fault structure of this region. Note that these boundary conditions are a simulation of the collision of Asia with the Indian subcontinent which produces mountain ranges (Himalayas) in front of the indenter and a penetrative deformation of Asia as far as 5000 km northward of the India-Asia boundary. Experiments of the kind presented here have been scaled down to represent the mechanics of the lithosphere[11] in order to study fault patterns observed at the Earth's surface.

Experiment 1 is shown in Fig. 1 and its digitized version in Fig. 2(a). One can observe a very broad size distribution of fracture regions. Two main fault directions (northeast and northwest) are present which are compatible with that of the northward maximum principal stress axis σ_1 (parallel to the direction of indentation) and that of the eastward minimum principal stress axis σ_3 (perpendicular to the free boundary). More precisely, they are tilted by an angle $\pm(\pi/4-\phi/2)$, where $\tan\phi = k$ ($=0.6$) is the coefficient of the frictional law. The northeastward fault family directly ensures lateral escape of a triangular block (the southeast corner of the sample). The conjugate (northwestward) family develops an antithetic motion compatible with the escape by

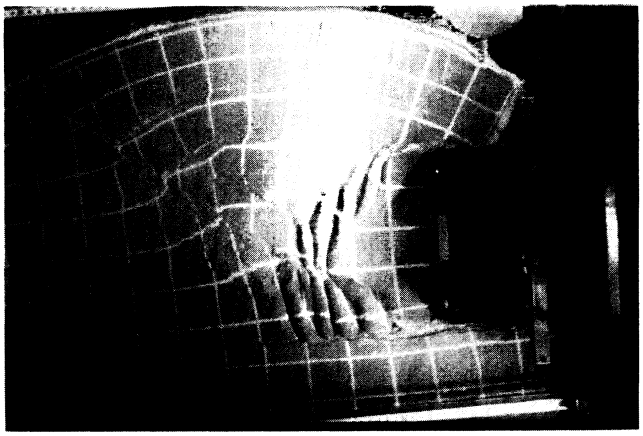

FIG. 1. Top view of experiment 1 and its setup. The rectangular wedge has penetrated over a distance of 15 cm in an initially undeformed system. The deformed array of white passive markers was initially a perfect square lattice. The free boundary on the right was initially a straight line 10 cm away from the indenter. The parameters of the experiment are as follows: upper brittle layer (sand) of thickness $=0.5$ cm, density $=1.2$; upper silicone of thickness $=0.5$ cm, density $=1.2$, viscosity $=0.6\times10^4$ Pas; lower silicone of thickness $=0.5$ cm, density $=1.4$, viscosity $=7\times10^4$ Pas; golden syrup of thickness $=5$ cm, density $=1.47$, viscosity $=100$ Pas.

counterclockwise rotations (so-called bookshelf[13]). One can identify a hierarchy of conjugate fault pairs forming Λ-shaped domains of decreasing size.

In order to explore the self-similarity of the observed fault pattern, we have applied a fractal analysis to the digitalized version Fig. 2(a) of the photograph shown in Fig. 1. We measure the total length $L(r)$ of the faults in a box of size $r\times r$ centered on a point belonging to a fault. Our algorithm first determines the position of the two ends of each fault, from which its length is computed. $L(r)$ is then obtained by summing all fault lengths within the box of size $r\times r$. Averaging over typically 100 different points inside the fault pattern, we obtain that the total length $L(r)$ can be fitted by $L(r)\sim r^{D_f}$ with a fractal dimension $D_f=1.74\pm0.05$. We have also measured the distribution $P(l)$ of faults of length l out of a total number of 135 digitalized faults. It can be fitted by the expression $P(l)\sim l^{-a}$, with an exponent $a=2.0\pm0.1$. Both power laws hold for r (l) in the range 0.3–10 cm (1–10 cm). The upper cutoff comes from the finite size of the indenter ($\Lambda=20$ cm). The lower cutoff $l_{\min}$ is controlled by the finite thickness h of the brittle layer and by the finite resolution of the digitizing process. This comes from the fact that most faults nucleate at the brittle-ductile interface, as demonstrated from x-ray-tomography studies.[14] Therefore, a fault will be observed only when its length is larger than h.

Other experiments have been performed under different brittle-ductile conditions. Figure 3 presents the results of experiment 2, performed under the same boundary condition as in Figs. 1 and 2 but with more viscous ductile layers. One can observe that the fault pattern is denser than in Figs. 1 and 2(a). Other experiments confirm that the higher the viscosity of the ductile layers, the denser the fault pattern.[12] Note that this is not in contradiction with our observation that D_f remains approximately constant since D_f measures only the *relative* self-similarity of the fault pattern and not the absolute number of faults or absolute total fault length. The geometry and fault density come from the coupling between the brittle and ductile layers and their opposite mode of deformation. The brittle layer responds to an applied strain by the development of faults since it cannot deform by more than 10% without creating a fault. The ductile layers tend to smooth out the velocity discontinuities associated with faults. As a result, in the small-viscosity cases, one expects and observes (see, for example, Fig. 1) the appearance of a few long faults presenting large offsets. The existence of a relatively large number of additional smaller faults may be attributed to deformation compatibility requirements (see below). In the large-viscosity cases, large offsets are forbidden by the viscous coupling. The strain is then accommodated by many faults with small offsets.

In Fig. 3, as in the previous case shown in Figs. 1 and 2, one can notice a hierarchy of fault lengths and Λ-shaped fault pairs for two different displacements of the

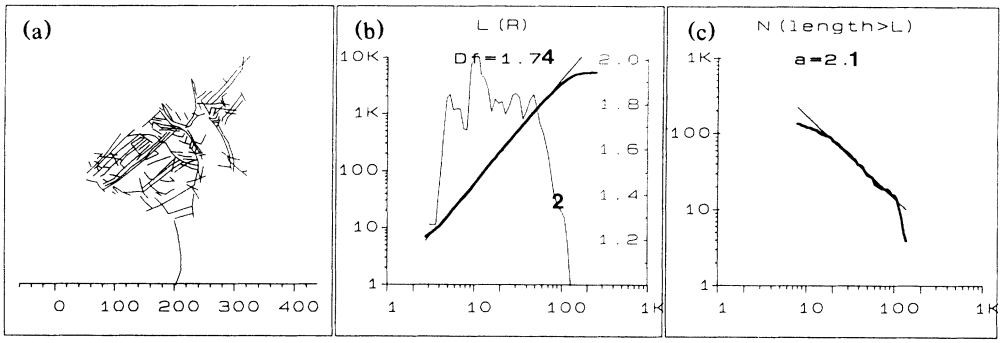

FIG. 2. Analysis of the fault pattern obtained in Fig. 1. (a) Digitized fault pattern; lengths are given in millimeters, i.e., 100 corresponds to 100 mm. (b) Logarithm of the total length $L(r)$ (in millimeters) of faults in a box size $r\times r$ as a function of log$r$ (r is given in millimeters). $L(r)$ is fitted by $L(r)\sim r^{D_f}$ (thin line) with $D_f=1.74\pm0.05$. The curve denoted 2 gives the local value of the slope (read on the scale on the right) of the log-log representation of $L(r)$. It gives an estimate of the uncertainty attached to D_f. (c) The number of faults $N(l)=\int_l^\infty P(l')dl'$ of length larger than l (in millimeters), fitted by $N(l)\sim l^{-a+1}$, with $a=2.1\pm0.1$.

indenter. The fractal dimension D_f is found to be essentially constant around 1.7. However, the fault-length distribution $P(l)$ changes with time. Over roughly a decade, $P(l)$ can be fitted by a power law $P(l)\sim l^{-a}$, with an exponent a decreasing from 2.5 ± 0.2 [Fig. 3(a)] to 2.0 ± 0.2 [Fig. 3(b)]. This reflects the growth of large faults at the expense of smaller faults fusing together.

These experimental results allow us to understand the main roles of the ductile layers. (1) Viscous stresses are small at larger scales ($\eta\,\partial v/\partial x\approx 1$–$10$ Pa for our typical viscosity and wedge velocity $v\approx 5$ cm/h over a distance of the order of 10^{-1} m) compared to mechanical stresses in the upper brittle sand layer (typically of the order of $\rho gh\approx 10^2$ Pa, where g is the gravitational acceleration, $h\approx 10^{-2}$ m is the thickness of the sand layer, and $\rho\approx 2000$ kg m^{-3} is the density of sand). Therefore, silicone layers ensure free boundary conditions under the sand layer, which is an essential condition for the properties that we report. However, at small scales ($\approx 10^{-3}$–10^{-2} m), viscous stress dominates and prevents velocity discontinuities. This explains the difference in fault patterns at small scales when varying the silicone viscosity. (2) The sandwich structure of the sand-silicone system favors in-plane two-dimensional shear rupture compared to three-dimensional thickening (which is only observed near the penetrating wedge). Indeed, thickening must overcome the *total* gravity force which increases with the *total* thickness of the system, whereas 2D shear rupture occurs when the shear stress is larger than a threshold which is a function only of the sand thickness.

In order to rationalize these results, one needs to know (1) the constitutive mechanical equations governing the deformation field, (2) the boundary conditions on the border of the system and on the growing structure (faults), (3) the rate of growth of the faults in relation to the deformation field, and (4) the nature of the disorder if any. We now discuss these points successively.

(1) We first propose to reduce the complexity of the full mechanical equations by focusing on the 2D kinematics only, namely, on the constraints applying to the deformation field. We note first the essential role played by the silicone layers which ensure that the deformations are two dimensional except near the wedge. A given deformation can be decomposed into pure shear strain, rigid-body rotations ω, and isotropic strain ε (corresponding to a change of surface associated with pure compression or extension). The rotation field ω plays an essential role in the structuration of the fault pattern via

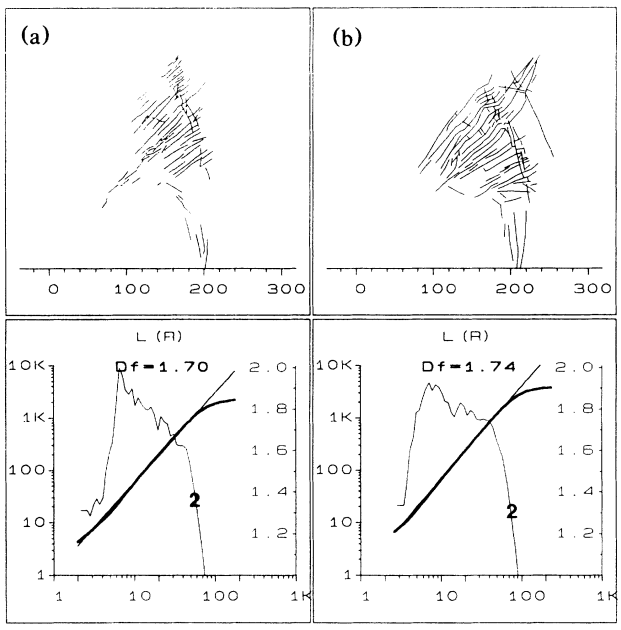

FIG. 3. Two stages of experiment 2 corresponding to the following parameters: same as in Fig. 1 except for viscosity $=2.3\times10^4$ Pa s for the upper silicone layer, and lower silicone of thickness $=1$ cm, density $=1.4$, and viscosity $=4.5\times10^4$ Pa s. The same unit of length (millimeter) as in Fig. 2 is used. (a) 12.5 cm and (b) 20 cm of indentation. In each case, the digitized fault pattern is shown with the cumulative length $L(r)$ defining the fractal dimension: (a) $D_f=1.70\pm0.05$ and (b) $D_f=1.74\pm0.05$.

the bookshelf mechanism.[13] The isotropic strain ε controls the pressure which itself affects the Mohr-Coulomb rupture criterion. Also, the corners of the Λ-shaped domains, recognized previously as the building blocks of the fractal fault pattern, are the loci of high three-dimensional compressive strain inside, due to the motion of the two border conjugate faults. It is thus natural to expect that ω and ε should play an important role in the formation of fault patterns. Indeed, it can be shown that the compatibility requirement between the various displacement gradients at each point of the system can be formulated explicitly within differential geometry and leads to second-order differential equations[15,16] relating rotation, isotropic, and shear deformations. In particular, the two fields ε and ω satisfy exactly the Laplace equation $\nabla^2 V=0$ (for $V=\varepsilon$ or ω) in the variables (x_i,y_i) which are connected to (x,y) by $(dx_i,dy_i)=A(dx,dy)$, where A is the displacement-gradient tensor associated with the isochoric part of the deformation.[15] In this local frame (x_i,y_i), nonisotropic deformations are removed which allows approximate preservation of the position of the barycenter and the direction of the principal axis of the fault pattern during the growth process. Note that the compatibility equations generalize to nonelastic materials the equation $\nabla^2 \mathrm{div}\,\mathbf{u}=0$ in elastic materials,[16] where $\mathbf{u}$ is the local deformation vector. The Laplace equation describes the existence of long-range correlations: For instance, once a fault is created, the stress and strain fields are redistributed over large distances (meaning algebraic decay of the stress) with stress enhancement at the tips.

(2) The boundary conditions are of mixed nature: The deformation is imposed on the penetrating wedge and must vanish on the rigid borders, whereas the stress is almost zero in the free east border. On a fault, there is a discontinuity of the displacement on both of its sides in a direction parallel to it, whereas displacements orthogonal to the fault are continuous in the absence of uplifting, overlapping, or void creation. Associated with this strain discontinuity, the shear stress along a fault is decreased. Even if this shear stress does not strictly vanish due to a remanent friction along the fault, this condition is similar to that of vanishing of the electrical current flux normal to a crack in the dual dielectric-breakdown model (DBM).[4] "Dual" refers to the transformation (current↔voltage), (resistance↔conductance), and (horizontal↔vertical) boundary conditions. Note that the creation of a fault entails a spatial redistribution of stress and strain induced by the stress drop associated with faulting, in a way analogous to the redistribution of currents in the DBM.

(3) A fault is created as soon as both following criteria are fulfilled: (i) a sufficient shear deformation (larger than 10% for sand) and (ii) a ratio of the shear stress over normal stress larger than the friction coefficient k. One thus expects that the rate of fault formation increases with the rate of deformation within the system.

(4) Finally, the source of "noise" can be found in small-scale imperfections in sample preparation in both the sand and silicone layers.

The analogies between these four ingredients and those entering in the DBM model are not sufficient to prove that both problems belong to the same universality class as suggested from the measured value of the fractal dimension, which is very close to that of DLA and DBM. The morphologies of the growth pattern are different, essentially due to the possibility for faults to develop unconnected to previous ones. The difference may also be attributed to the fact that under the change of reference frame from (x,y) to (x_i,y_i), the metric properties are not conserved locally which implies that the morphologies are distorted inhomogeneously under the frame transformation. However, the hierarchy of Λ-shaped domains is reminiscent of the branching process of DLA growth. In the future, we hope to clarify the relation with DLA growth processes which has been only suggested here, and to study the respective roles of the different ingredients of the model.

[1]T. A. Witten and L. M. Sander, Phys. Rev. Lett. **47**, 1400 (1981).

[2]See, for example, S. Tolman and P. Meakin, Phys. Rev. A **40**, 428 (1989), and references therein.

[3]L. M. Sander, Nature (London) **322**, 789 (1986).

[4]N. Niemeyer, L. Pietronero, and H. J. Weismann, Phys. Rev. Lett. **53**, 1023 (1984).

[5]M. Sahimi and J. D. Goddard, Phys. Rev. B **33**, 7848 (1986); S. Arbabi and M. Sahimi, Phys. Rev. B **41**, 772 (1990); L. de Arcangelis, A. Hansen, H. J. Herrmann, and S. Roux, Phys. Rev. B **40**, 177 (1989).

[6]H. J. Herrmann, in *Random Fluctuations and Pattern Growth: Experiments and Models,* edited by H. E. Stanley and N. Ostrowsky, NATO Advanced Study Institute Vol. 157 (Kluwer Academic, Dordrecht, 1988), p. 149.

[7]G. Mandl and R. Fernandez Luque, Geotechnique **20**, 277 (1970).

[8]*Fractals in Geophysics,* edited by C. H. Scholz and B. B. Mandelbrot (Birkhaüser Verlag, Stuttgart, 1989); B. B. Mandelbrot and B. H. Kaye, *A Random Walk through Fractal Dimensions* (VCH, Weinheim, 1989).

[9]*Fracture Mechanics of Rocks,* edited by B. K. Atkinson (Academic, New York, 1987).

[10]P. Tapponnier, G. Peltzer, and R. Armijo, in *Collision Tectonics,* edited by M. P. Coward and A. C. Ries [Geol. Soc. Spec. Publ. (London) **19**, 115 (1986)].

[11]P. Davy and P. R. Cobbold, Bull. Geol. Inst. Univ. Uppsala **14**, 129 (1988).

[12]P. Davy, A. Sornette, and D. Sornette (to be published).

[13]D. P. McKenzie and J. A. Jackson, J. Geol. Soc. (London) **143**, 349 (1986); see also G. Mandl, Tectonophysics **141**, 277 (1987).

[14]P. Richard, J. F. Ballard, B. Colletta, and P. Cobbold, C. R. Acad. Sci. (Paris) **309**, 2111 (1989).

[15]P. R. Cobbold, Tectonophysics **39**, T1 (1977).

[16]L. Landau and E. Lifschitz, *Theory of Elasticity* (Mir, Moscow, 1967).

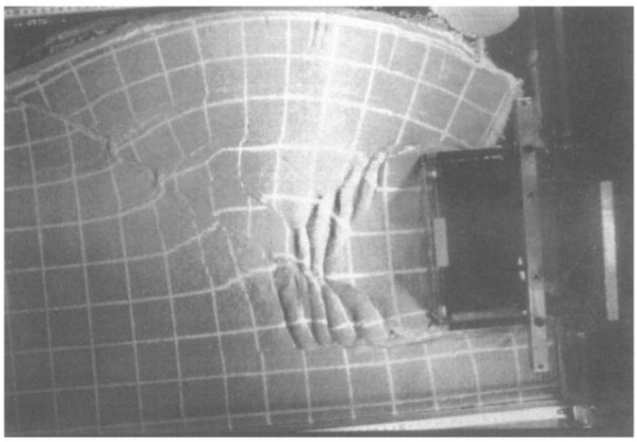

FIG. 1. Top view of experiment 1 and its setup. The rectangular wedge has penetrated over a distance of 15 cm in an initially undeformed system. The deformed array of white passive markers was initially a perfect square lattice. The free boundary on the right was initially a straight line 10 cm away from the indenter. The parameters of the experiment are as follows: upper brittle layer (sand) of thickness = 0.5 cm, density = 1.2; upper silicone of thickness = 0.5 cm, density = 1.2, viscosity = 0.6×10^4 Pa s; lower silicone of thickness = 0.5 cm, density = 1.4, viscosity = 7×10^4 Pa s; golden syrup of thickness = 5 cm, density = 1.47, viscosity = 100 Pa s.